An *in Situ* Infrared Study of Dimethyl Carbonate Synthesis from Carbon Dioxide and Methanol over Zirconia

Kyeong Taek Jung and Alexis T. Bell[1]

*Chemical Sciences Division, Lawrence Berkeley Laboratory and Department of Chemical Engineering,
University of California, Berkeley, California 94720-1462*

The mechanism of dimethyl carbonate (DMC) synthesis from methanol and carbon dioxide over monoclinic zirconia has been investigated using *in situ* infrared spectroscopy. The dissociative adsorption of methanol occurs more slowly than the adsorption of carbon dioxide, but the species formed from methanol are bound more strongly. On adsorption, the oxygen atom of methanol binds to coordinately unsaturated Zr^{4+} cations present at the catalyst surface. Rapid dissociation of the adsorbed methanol leads to the formation of a methoxide group ($Zr–OCH_3$) and the release of a proton, which reacts with a surface hydroxyl group to produce water. Carbon dioxide inserts into the $Zr–O$ bond of the methoxide to form a mondentate methyl carbonate group ($Zr–OC(O)OCH_3$). It is proposed that this process is facilitated by the interactions of C and O atoms in CO_2 with Lewis acid-base pairs of sites ($Zr^{4+}O^{2-}$) on the surface of the catalyst. Methyl carbonate species can also be produced via the reaction of methanol with carbon dioxide adsorbed in the form of bicarbonate species, but this process is slower than that involving the reaction of carbon dioxide with methoxide species. DMC is formed by reaction of the methyl carbonate species with methanol, a process that results in the transfer of a methyl group to the carbonate and restores a hydroxyl group to the zirconia surface. The decomposition of DMC on monoclinic zirconia has also been investigated and has been observed to occur via the reverse of the processes described for the synthesis of DMC. © 2001 Elsevier Science

INTRODUCTION

Dimethyl carbonate (DMC) is a nontoxic molecule that can be used for a variety of applications. For example, DMC has been proposed as a methylating agent for aromatic compounds, to replace methyl halides and dimethyl sulfate, which are both toxic and corrosive, and as an intermediate in the synthesize polycarbonates and isocyanates, thereby avoiding the need to use phosgene (1, 2). DMC is also a candidate for replacing tertiary butyl ether (MTBE) as an oxygen-containing additive for gasoline (3). For these reasons, there has been a growing interest in examining novel approaches to the synthesis of DMC (1, 3).

Studies by Fujimoto and co-workers (4–6) have demonstrated recently that DMC can be synthesized by the reaction of methanol with carbon dioxide:

$$2\,CH_3OH + CO_2 \rightarrow (CH_3O)_2CO + H_2O.$$
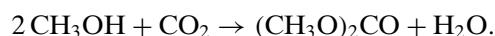
Of the various catalysts tested only ZrO_2 was found to be active. The effectiveness of this catalyst was attributed to the presence of both acidic and basic sites. It was proposed that basic sites are required to activate methanol and CO_2, and that acidic sites are required to supply methyl groups from methanol in the last step of the reaction mechanism (6). Based on evidence from infrared spectroscopy (6), it was proposed that methoxide species are formed on adsorption of methanol on basic sites and that these species are rapidly converted to methyl carbonate species. Methanol adsorption at acidic sites is thought to produce methyl carbocations, which then react with the anionic methyl carbonate to produce DMC. The general features of this mechanism are supported by *in situ* Raman studies of the reaction mechanism for both DMC formation and decomposition (7). Here we report a detailed investigation of the DMC synthesis over monoclinic zirconia (m-ZrO_2) undertaken for the purpose of identifying the nature of the reaction sites required for each step and the extent to which strongly and weakly adsorbed CO_2 are involved in the formation of methyl carbonate. *In situ* infrared spectroscopy was used to follow the dynamics of each reaction step.

EXPERIMENTAL

Monoclinic zirconia was prepared by boiling a 0.5 M solution of zirconyl chloride ($ZrOCl_2 \cdot 8H_2O$, Aldrich) under reflux at 373 K for 240 h, while maintaining the pH at 1.5. The precipitated material was recovered by vacuum filtration and washed repeatedly by redispersion in deionized water in order to remove chloride. After each wash, a few drops of $AgNO_3$ solution were added to the filtrate liquid. The washing process was repeated until no evidence for a precipitate of AgCl could be observed. The freshly prepared material was dried in air at 383 K and then calcined at

[1] To whom correspondence should be addressed. E-mail: bell@cchem.berkeley.edu.
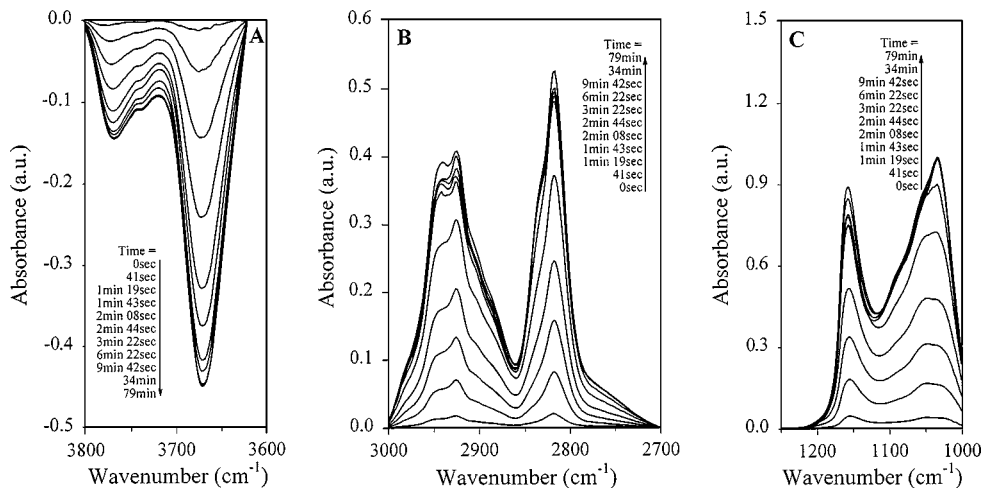
FIG. 1. Infrared spectra taken during exposure of m-ZrO$_2$ to CH$_3$OH at 298 K.

573 K for 3 h. The BET surface area of the calcined zirconia was 110 m^2/g. X-ray powder diffraction by powder diffractometry showed that only the monoclinic phase of zirconia was present in the calcined material.

In situ transmission infrared spectroscopy was performed using a 2-cm-diameter catalyst disk weighing 50 mg. The catalyst disk was contained in a low dead-volume infrared cell (8). Infrared spectra were collected using a Nicolet Magna 750 series II Fourier transform infrared spectrometer. Signals were detected using a narrow-band MCT detector. Satisfactory signal-to-noise was obtained by collecting 21–64 scans at 4 cm^{-1} resolution. Electrical resistance heaters were used to heat the cell and an Omega Series CN-2010 programmable temperature controller was used to control the cell temperature.

All gases were purified prior to use and delivered to the infrared cell via Tylan Model FC-280 mass flow controllers at a flow rate of 60 cm^3/min. He gas was passed through an oxysorb (CrO$_2$) trap to remove O$_2$ and then through a molecular sieve trap (3 Å Davison grade 564) to remove water. A He stream containing either 1% CO$_2$ or CH$_3$OH was used for studies of adsorption and reaction. DMC (0.01%) diluted in He was used to investigate the adsorption and decomposition of DMC.

RESULTS

Infrared spectra taken during the adsorption of methanol on zirconia at 298 K are illustrated in Fig. 1. In all cases the spectra are referenced to the spectrum of zirconia observed prior to the start of methanol adsorption. On adsorption, methanol reacts with the surface hydroxyl groups of zirconia to form methoxide groups with the concurrent release of water. Figure 1A shows the decrease in the absorbance of bands at 3768, 3745, and 3672 cm^{-1} associated with ter-

minal, bibridged, and tribridged OH groups, respectively, present on the surface of m-ZrO$_2$ (9–12). The growth in intensity of the bands at 2923 and 2817 cm^{-1}, associated with C–H stretching vibrations of monodentate and bidentate of methoxide groups, is seen in Fig. 1B and the growth in intensity of the bands at 1157 and 1032 cm^{-1}, associated with bending vibrations for both types methoxide groups, is seen in Fig. 1C (13–20). Bands can also be seen in Fig. 1B at 2943 and 2831 cm^{-1} for molecularly adsorbed CH$_3$OH [see (21, 22) and references therein] and at 2965 and 2881 cm^{-1} for bidentate formate species (15, 19, 23–32). The dynamics of OH group consumption and CH$_3$O group formation are presented in Fig. 2. The rates of hydroxyl group consumption and methoxide group formation are essentially
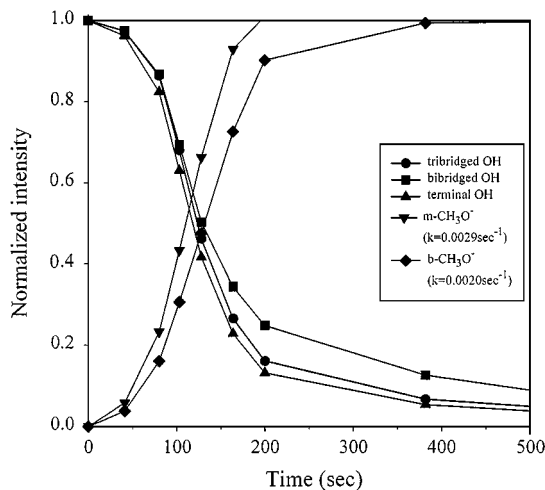
FIG. 2. Intensities of OHs and methoxy features for m-ZrO$_2$ taken during the experiments shown in Fig. 1. Band intensities are normalized to those observed at the beginning of the transient for hydroxyl groups, and to the values observed at the end of transient for methoxy groups.
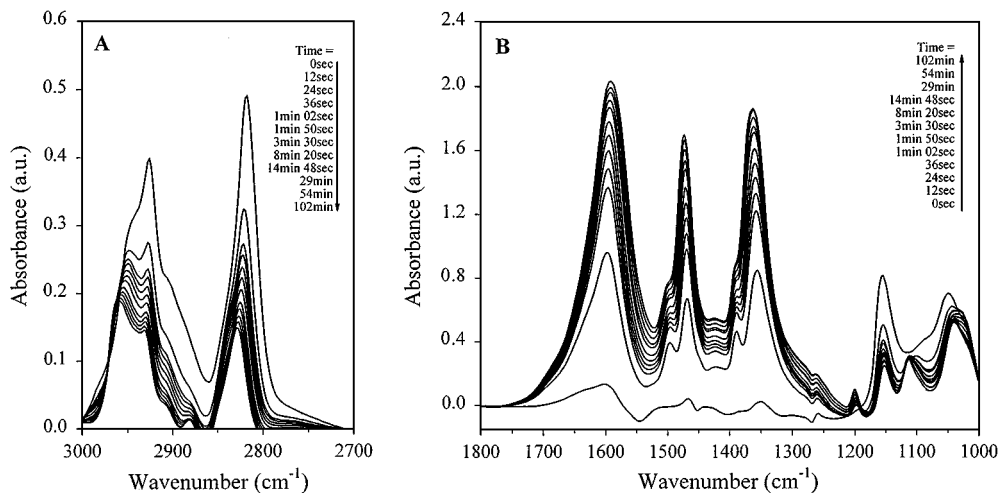
FIG. 3. Infrared spectra taken during exposure of m-ZrO_2 containing preadsorbed CH_3OH to CO_2 at 298 K.

equivalent. It is also evident that terminal and tribridged OH groups react at equivalent rates and that the rate of formation of m-CH_3O groups is slightly faster than the rate of formation of b-CH_3O groups. The apparent first-order time constant for the consumption of m-CH_3O–Zr species is 2.0×10^{-3} s^{-1} and that for b-CH_3O–Zr species is 2.9×10^{-3} s^{-1}.

The exposure of m-ZrO_2 containing methoxide groups to a stream of CO_2 in He results in a significant change in the appearance of the infrared spectrum of adsorbed species. As seen in Fig. 3B, the bands for m- and b-CH_3O (1157 and 1032 cm^{-1}) decrease and new features appear at 1600, 1497, 1474, 1389, 1370, 1200, and 1113 cm^{-1}. As indicated in Table 1, these features can be assigned to adsorbed monodentate methyl carbonate species (m-CH_3OCOO–Zr) based on the closeness of the band positions seen in Fig. 3 with those reported for methyl carbonate species associ-

ated with different metals (33, 34). It is also noted that the positions of the bands observed in Fig. 3 are nearly identical to those previously observed on ZrO_2 under similar conditions (see Table 1) (6, 10). Evidence for the formation of methyl carbonate species can also be obtained by examining the C–H stretching portion of the spectrum. As seen in Fig. 3A, with increasing exposure of the sample to CO_2, the bands for CH_3O–Zr species (2923 and 2817 cm^{-1}) decrease and new features appear at 2965 and 2883 cm^{-1}. This pattern is similar to that reported previously (6, 10), and as suggested by Table 1, the new features appearing in the spectrum are characteristic of m-CH_3OCOO–Zr. Figure 3A indicates that m-CH_3O species react more rapidly and extensively than do b-CH_3O–Zr species, and Fig. 4 shows that the dynamics of m-CH_3O consumption and m-CH_3OCOO–Zr formation are nearly identical. It is also evident that not all m-CH_3O–Zr species react at an equivalent rate, since

TABLE 1

Comparison of Bands Observed on Reaction of CO_2 with Adsorbed Zr–OCH_3 with Those for Monodentate Methyl Carbonate Species

Na–O(CO)OCH$_3$[a]	Sn–O(CO)OCH$_3$[b]	Pb–O(CO)OCH$_3$[b]	Zr–O(CO)OCH$_3$[c]	Zr–O(CO)OCH$_3$[d]	Zr–O(CO)OCH$_3$[e]
1631	1631	1623	—	—	—
1618	1610	1602	1583	1600	1600
1474	1453	1449	1478	1474	1474
1378	1372	1322	1372	1370	1389/1370
1193	1202/1190	1187	1223/1200	1223	1200
1100	1182	1165	1120	1112	1113
1090	1071	1092	—	—	—
935	937	925	943	—	900

Note. All frequencies shown in cm^{-1}.
[a] From Ref. (34).
[b] From Ref. (33).
[c] From Ref. (10).
[d] From Ref. (6).
[e] From this work.
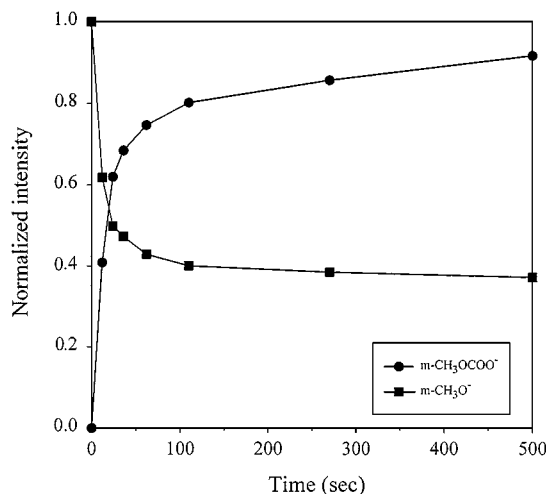
FIG. 4. Intensities of m-CH$_3$O–Zr and m-CH$_3$OCOO–Zr features for m-ZrO$_2$ taken during the experiments shown in Fig. 3. Band intensities are normalized to those observed at the beginning of the transient for m-CH$_3$O–Zr, and to the value observed at the end of transient for m-CH$_3$OCOO–Zr.

the rate of m-CH$_3$O–Zr consumption decreases rapidly and then much more slowly after about 60% of the original inventory of m-CH$_3$O has been consumed.

Infrared spectra taken during the exposure of the sample to CO$_2$ are shown in Fig. 5A. Bands rapidly appear at 1625, 1437, and 1225 cm^{-1}, characteristic of bidentate bicarbonate species (b-HCO$_3$–Zr), and a band at 1325 cm^{-1} is characteristic of bidentate carbonate species (b-CO$_3$–Zr) (12, 14, 15, 19, 23, 24, 35–39). As seen in Fig. 5B, the adsorption of CO$_2$ is very rapid and the apparent first-order rate coefficient is 3.2×10^{-2} s^{-1}.

Figure 6 illustrates the evolution of spectral features when ZrO$_2$ containing preadsorbed CO$_2$ is exposed to a

He stream containing CH$_3$OH. The bands associated with b-HCO$_3$–Zr (1625, 1437, 1330, and 1225 cm^{-1}) disappear within the first 40 s of CH$_3$OH exposure and new bands appear that are characteristic of m- and b-CH$_3$O–Zr (1157 and 1032 cm^{-1}, respectively) and of m-CH$_3$OCOO–Zr (1608, 1464, and 1340 cm^{-1}). A band is also seen at 1530 cm^{-1}, even after exposure of the sample to CH$_3$OH for 2 days. This feature is best assigned to bidentate carboxylate species (b-CO$_2$–Zr). Comparison of Figs. 2 and 6 indicates that the intensities of the bands for m-CH$_3$OCOO–Zr are considerably lower when this species is formed via the reaction of CH$_3$OH with adsorbed CO$_2$.

The spectrum of adsorbed species evolves in a complex fashion when a mixture of CH$_3$OH and CO$_2$ are passed over the catalyst surface. Figure 7A shows that in the first few seconds of exposure at 298 K, the only features seen are those for b-HCO$_3$–Zr (1625, 1450, and 1225 cm^{-1}) and b-CO$_3$–Zr (1325 cm^{-1}). The rapid appearance of these species is attributable to the rapid rate of CO$_2$ adsorption, which is tenfold faster than the rate of CH$_3$OH adsorption. With increasing time, the bands for b-HCO$_3$–Zr and b-CO$_3$–Zr are replaced by those characteristic of m- and b-CH$_3$O–Zr (1157 and 1032 cm^{-1}) and m-CH$_3$OCOO–Zr (1600, 1497, 1474, 1389, 1370, 1200, and 1113 cm^{-1}). Figure 7B shows that the same pattern is observed at 423 K, the principal differences being that at the higher temperature the rate of appearance of m-CH$_3$OCOO–Zr is faster and the ratio of m-CH$_3$O–Zr to m-CH$_3$OCOO–Zr is higher than at the lower temperature.

Figure 8 shows the changes occurring in the intensity of bands for m-CH$_3$O–Zr and m-CH$_3$OCOO–Zr as functions of time under different circumstances. In each case, the surface concentration of m-CH$_3$OCOO–Zr was achieved by exposing m-ZrO$_2$ to a mixture containing CH$_3$OH and CO$_2$. When the initial gas mixture was swept out with He,
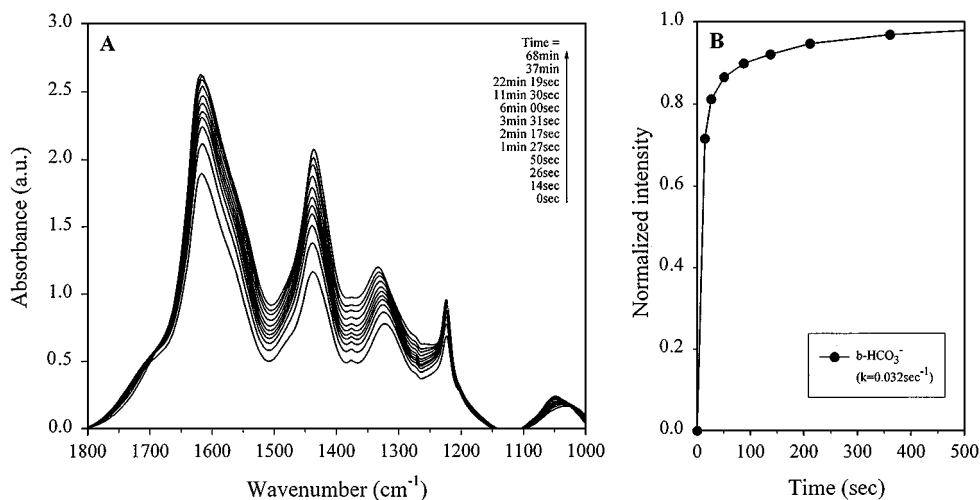
FIG. 5.   Infrared spectra taken during exposure of m-ZrO$_2$ to CO$_2$ at 298 K.
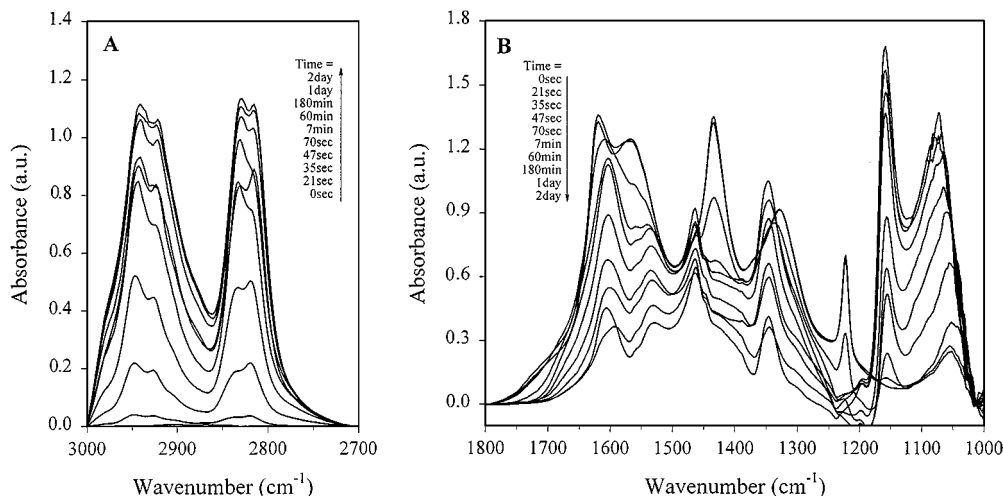
FIG. 6. Infrared spectra taken during exposure of m-ZrO_2 containing preadsorbed CO_2 to CH_3OH at 298 K.

the initial concentration of m-CH_3OCOO–Zr declined toward zero, whereas the concentration of m-CH_3O–Zr increased relative to its initial value. When the mixture of CH_3OH and CO_2 was swept out with CO_2, the surface concentration of m-CH_3OCOO–Zr grew, whereas the surface concentration of m-CH_3O–Zr declined. A rapid decrease in the surface concentration of m-CH_3OCOO–Zr occurred when the initial gas mixture was swept out with CH_3OH. This change was accompanied by an increase in the surface concentration of m-CH_3O–Zr. A qualitatively similar pattern was observed at 423 K, a temperature very close to that at which the formation of DMC over ZrO_2 is reported to be a maximum (6). In this case, though, the rates of m-CH_3OCOO–Zr disappearance in He and CH_3OH are comparable. It is also noted that raising the temperature increases the former process to a much greater degree than the latter.

FIG. 7. Infrared spectra taken during exposure of m-ZrO_2 to the mixture of CO_2 and CH_3OH at (A) 298 K and (B) 423 K.
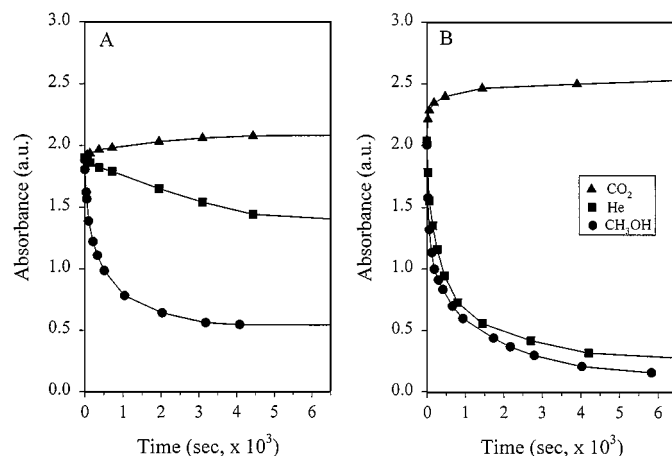
FIG. 8. Intensities of m-CH_3OCOO–Zr for m-ZrO_2 taken after switching from a mixture of CO_2 and CH_3OH to a mixture of CH_3OH, CO_2, and He at (A) 298 K and (B) 423 K.
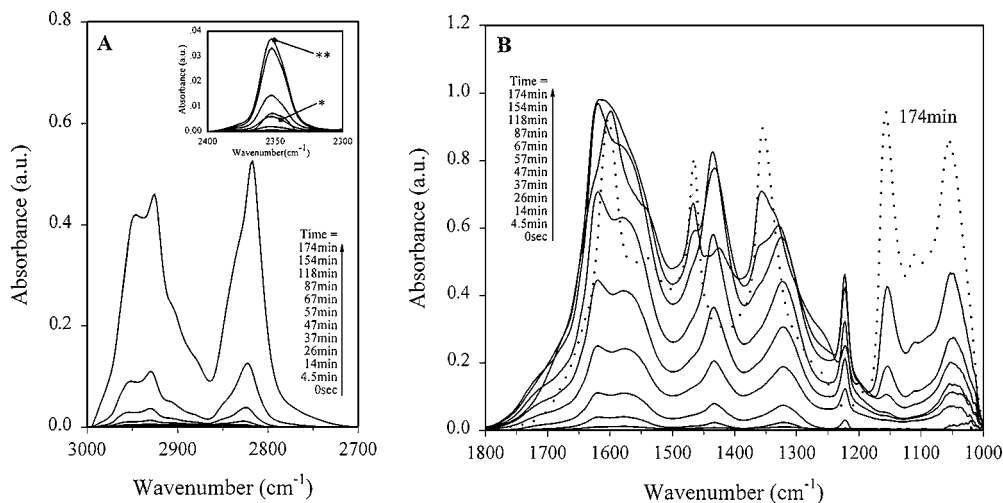
FIG. 9. Infrared spectra taken during the exposure of m-ZrO_2 to DMC at 298 K. Four distinguishable features shown in panel A were obtained from exposure times of 87–174 min. The inset shows that the peak at 2350 cm^{-1} increased with the exposure time from 57 min (*) to 87 min (**) and then decreased.

The series of spectra shown in Fig. 9 were obtained on exposure of the sample to a gas stream containing DMC. At low exposure times (<67 min) the only features observed in Fig. 9B are those for b-HCO_3–Zr and b-CO_3–Zr species. However, as the exposure time increases, the spectrum evolves and ultimately becomes characteristic of that for a mixture of m-CH_3OCOO–Zr and m- and b-CH_3O–Zr. Comparison of the last spectrum in the sequence appearing in Fig. 9 with that appearing at long times in either Fig. 3 or 6 shows that they are essentially identical, the only difference being that the intensities of the peaks associated with m-CH_3OCOO–Zr are smaller in Fig. 9. The transient evolution of CO_2 is also observed, as evidenced by the appearance of a weak band at 2350 cm^{-1}, as seen in Fig. 9A. Figure 10 shows a plot of band intensities versus the time of exposure of m-ZrO_2 to DMC.
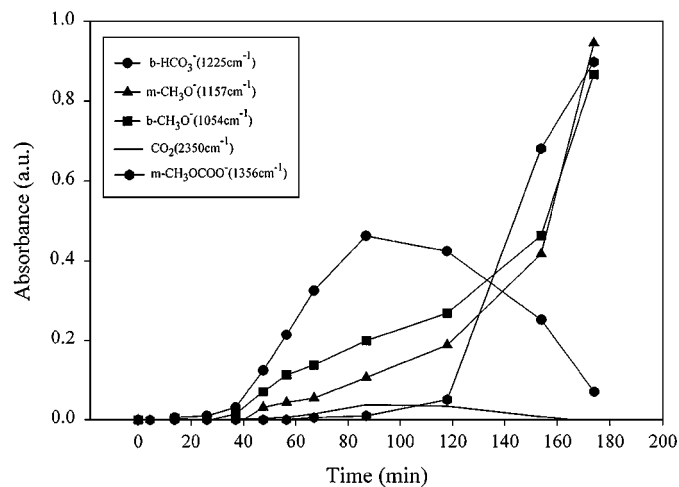
FIG. 10. Plot of band intensities taken during exposure of m-ZrO_2 to DMC at 298 K.

DISCUSSION

The interactions of CH_3OH with the surface of ZrO_2 reported in the present study are qualitatively consistent with those described previously (6, 7, 10). It is envisioned that the initial adsorption of CH_3OH on m-ZrO_2 occurs via the interaction of the O atom of CH_3OH with a coordinately unsaturated Lewis acid Zr^{4+} center on the surface of m-ZrO_2. This interaction can then result in the transfer of the H atom associated with the OH group of the alcohol to a coordinately unsaturated O^{2-} center on the surface of m-ZrO_2 or reaction with a surface OH group. The first of these two cases would result in the formation of bridging (tri- or bibridging) OH group and a methoxide group, whereas the latter case would result in the release of water and the formation of a methoxide group. Figure 2 shows that the disappearance of surface OH groups and the appearance of CH_3O–Zr groups are preceded by a short induction period, after which the dynamics of the two processes are virtually identical. This suggests that the formation of CH_3O–Zr groups and the release of H_2O occur concurrently. Therefore the overall process can be described as in Scheme 1.

As was noted above, the rates of consumption of terminal and tribridging OH groups is identical and, correspondingly, so are the rates of formation of monodentate (terminal) and bidentate (bridging) CH_3O–Zr groups.
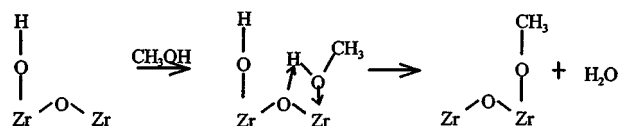
SCHEME 1

The changes in the infrared spectrum observed when methoxide groups interact with CO_2, shown in Fig. 3, are qualitatively similar to those reported earlier for similar interactions occurring over both ZrO_2 (6, 7, 10) and Al_2O_3 (40). Also in agreement with previous results is the observation that m-CH_3O–Zr species are more reactive than b-CH_3O–Zr species (10). While the insertion of CO_2 into metal–hydrogen, metal–carbon bonds, and metal–nitrogen bonds of various compounds is well-known, the analogous insertion of CO_2 in M–OR bonds has few documented precedents (41). An exception, though, is a recent description of CO_2 insertion into the M–OCH_3 bonds of methoxide-containing complexes based on Mg or Ca (42). The site requirements and the mechanism of CO_2 insertion into metal alkoxide bonds are also poorly understood. It has been proposed that the first step in the insertion of CO_2 into a Zr–OCH_3 bond involves an electron donor–acceptor interaction in which the alkoxy oxygen lone pairs act as the donor and the CO_2 carbon atom as the acceptor (10). A more likely scenario is that several donor acceptor interactions occur simultaneously, as suggested in Scheme 2.

In this instance a coordinately unsaturated surface oxygen atom donates charge to the carbon atom of CO_2, and concurrently, an oxygen atom of CO_2 donates charge to the Zr^{4+} cation to which the methoxide group is attached. The proximity of the methoxide oxygen atom to the CO_2 carbon atom would then enable the transfer of the alkoxide group to the carbon atom of CO_2 and the simultaneous formation of a Zr–O bond between the Zr^{4+} cation and one of the oxygen atoms of CO_2. The formation of m-CH_3OCOO–Zr species, as opposed to bridging, chelating, or chelating bridging methyl carbonate species, is suggested by the close agreement between the observed infrared bands and the positions of the bands in well-defined methyl carbonate compounds, as shown in Table 1. It should be noted that the reaction in Scheme 2 is readily reversible. As shown in Fig. 8, in the absence of gas-phase CO_2, m-CH_3OCOO–Zr decomposes to release CO_2 and produce m-CH_3OH–Zr.

In a previous study, we suggested on the basis of evidence from Raman spectroscopy that methyl carbonate species are formed on the surface of ZrO_2 via the reaction of bicarbonate species with methoxide species (7). The experiment shown in Fig. 6 was undertaken in an effort to confirm the occurrence of this process. As was already noted, the results of this experiment are difficult to interpret, since several processes appear to take place concurrently. The
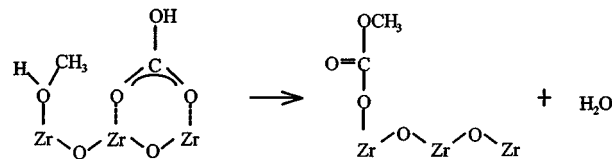
SCHEME 3

appearance of bands at 1608, 1464, 1340, and 1200 cm^{-1} does confirm the formation of m-CH_3OCOO–Zr species, but the intensity of these bands is considerably smaller than those seen when methoxide groups are allowed to interact with CO_2. The appearance of a broad band in the region of 1540–1550 cm^{-1} suggests that b-CO_3–Zr species may be formed, possibly by transfer of an H atom from HCO_3–Zr to either methanol or a methoxide species. Thus, it is possible to envision a pathway to m-CH_3OCOO–Zr from b-HCO_3–Zr, as shown in Scheme 3.

This reaction appears to occur much more slowly than that in Scheme 2. It is also interesting to observe that the preexistence of b-HCO_3–Zr species leads to an increase in the surface concentration of b-CH_3O–Zr relative to m-CH_3O, the more reactive form of methoxide. The reason for this is most likely that b-HCO_3–Zr species are bound in a chelating manner to a single Zr^{4+} cations, thereby decreasing the availability of sites for the stabilization of m-CH_3O–Zr species, a phenomenon similar to that reported for formate groups (43).

The experiments in which CH_3OH and CO_2 are passed concurrently over the catalyst also support the hypothesis that methyl carbonate species are formed predominantly via CO_2 addition to methoxide species. Figure 7 shows convincingly that while the initial adsorbed species are b-HCO_3–Zr because of the more rapid adsorption of CO_2 than CH_3OH, as soon as methoxide species are formed they rapidly react with CO_2 to form m-CH_3OCOO–Zr species. This suggests that under steady state reaction conditions the primary route to methyl carbonate species will be the reaction in Scheme 2.

The elementary process via which DMC is formed from methyl carbonate species cannot be identified by direct evidence. As seen in Fig. 8, exposure of m-CH_3OCOO–Zr species to methanol results in a rapid loss of these species without the formation of any new intermediates. The presence of DMC in the gas phase in such experiments could not be detected because of the very low concentration of the products. Thus, one can only infer that DMC is formed via reaction of CH_3OH with m-CH_3OCOO–Zr. This conclusion is supported, though, via the concept of microreversibility, which requires that the decomposition of DMC occur via the same elementary steps by which it forms. Based on this logic, the first step of DMC decomposition
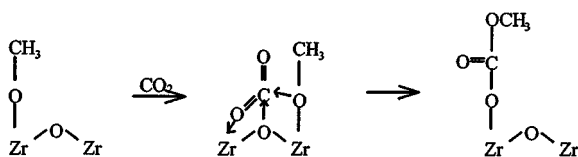
SCHEME 2
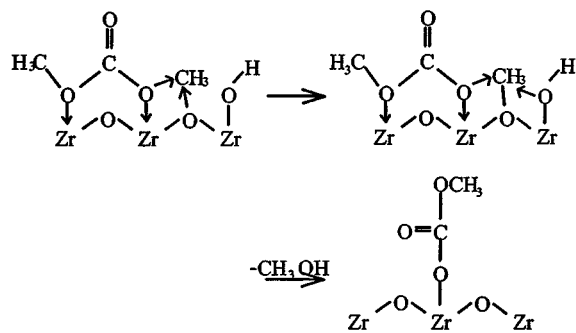
SCHEME 4

and the last step of DMC formation should represent the forward and reverse directions of the same elementary step. In addition, reference to Fig. 8A indicates that the loss of m-CH_3OCOO–Zr from the catalyst surface when it is exposed to a stream containing CH_3OH in He is an order of magnitude more rapid than when the stream only contains He. From this is inferred that the addition of a methyl group from adsorbed CH_3OH (see Fig. 9) is faster than the decomposition of m-CH_3OCOO–Zr to release CO_2.

In Fig. 9 it was shown that the adsorption of DMC on m-ZrO_2 results in the appearance initially of b-HCO_3 and weakly bound CO_2. With increasing time, both of these species disappear and new features appear for m-CH_3OCOO–Zr and m- and b-CH_3O–Zr. This pattern can be explained as follows. On adsorption, DMC dissociates rapidly to form methoxide species and gas-phase CO_2. A part of the latter species is readsorbed as b-HCO_3–Zr. The initially formed methoxide groups are not observed because they react very rapidly with small amounts of water vapor held by the catalyst. Previous studies have shown that methoxide species on the surface of ZrO_2 will react very rapidly with water vapor at 298 K to form methanol. Once the water vapor supply has been exhausted, methoxide species build up on the catalyst surface and so does the inventory of m-CH_3OCOO–Zr. This scenario suggests that on adsorption DMC forms a bidentate methyl carbonate group and transfers a methyl group to a bridging O atom on the surface of ZrO_2. The methyl group reacts, in turn, with a hydroxyl group to form methanol and desorbs from the surface (Scheme 4).

The residual methyl carbonate species isomerizes to the monodentate structure and then decomposes to a CH_3O–Zr species, with the concurrent release of CO_2. Water ad-
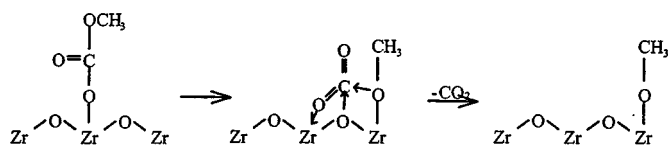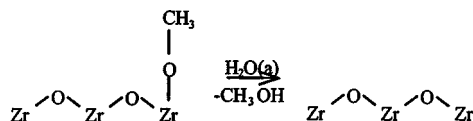
SCHEME 6

sorbed on the surface of ZrO_2 would rapidly react with the CH_3O–Zr species to produce CH_3OH and hydroxyl species. Such a scenario is quite plausible, since the adsorption energy of water is relatively high [15–30 kcal/mol (44, 45)] and CH_3O–Zr species have been observed to react very rapidly with water at 298 K (19, 20). Once the supply of adsorbed water is exhausted CH_3O–Zr species are retained on the catalyst surface and further decomposition of CH_3COO–Zr is halted (Schemes 5 and 6).

CONCLUSIONS

The mechanism of DMC synthesis can be envisioned to occur via the sequence of steps shown in Fig. 11. Methanol binds to Zr^{4+} Lewis acid sites and releases an H atom, which then rapidly reacts with a surface OH group to form H_2O. CO_2 is then inserted into the Zr–O bond of the CH_3O–Zr species to produce m-CH_3OCOO–Zr. This process is facilitated by interactions of C and O atoms in CO_2 with Lewis acid–base pairs of sites. Methyl carbonate species can also be produced via the reaction of CH_3OH with CO_2 adsorbed in the form of bicarbonate species, but this process is slower than that involving the reaction of CO_2 with methoxide species. DMC is formed by transfer of a methyl group to the terminal O atom of methyl carbonate species.
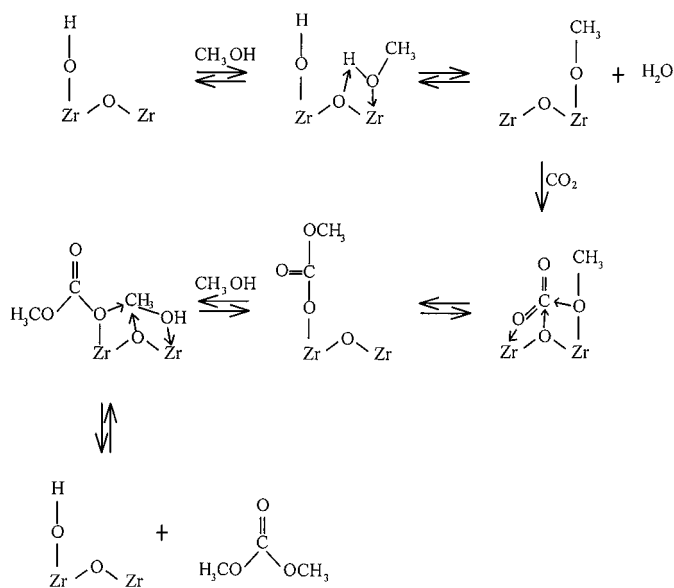
FIG. 11. Proposed mechanism for the formation of DMC from CO_2 and CH_3OH.

SCHEME 5

The effectiveness of ZrO_2 as a catalyst for the synthesis of DMC from CH_3OH and CO_2 stems from the presence of amphoteric Zr–OH hydroxyl groups and coordinately unsaturated $Zr^{4+}O^{2-}$ sites that act as Lewis acid–base pairs.

ACKNOWLEDGMENT

REFERENCES

1. Ono, Y., *Catal. Today* **35**, 15 (1997).
2. Antas, P. T., and Williams, T. C., "Green Chemistry—Frontiers in Benign Chemical Syntheses and Processes." Oxford, New York, 1998.
3. Pacheco, M. A., and Marshall, C. L., *Energy Fuels* **11**, 2 (1997).
4. Fang, S., and Fujimoto, K., *Appl. Catal. A* **142**, L1 (1996).
5. Tomishige, K., Sakaihori, T., Ikeda, Y., and Fujimoto, K., *Catal. Lett.* **58**, 225 (1999).
6. Tomishige, K., Ikeda, Y., Sakaihori, T., and Fujimoto, K., *J. Catal.* **192**, 355 (2000).
7. Xie, S., and Bell, A. T., *Catal. Lett.* **70**, 137 (2000).
8. Hicks, R. F., Kellner, C. S., Savatsky, B. J., Hecker, W. C., and Bell, A. T., *J. Catal.* **71**, 216 (1981).
9. Tsyganenko, A. A., and Filimonov, V. N., *J. Mol. Struct.* **19**, 1183 (1979).
10. Benestil, M., Moravek, V., Lamotte, J., Saur, O., and Lavalley, J. C., *Spetrochim. Acta A* **43**, 1487 (1987).
11. Kondo, J., Domen, K., Maruya, and Onishi, T., *Chem. Phys. Lett.* **188**, 443 (1990).
12. Jung, K. T., and Bell, A. T., *J. Mol. Catal.* **163**, 7 (2000).
13. He, M. Y., and Ekerdt, J. G., *J. Catal.* **184**, 357 (1984).
14. Kondo, J., Abe, H., Sakata, Y., Maruya, K., Domen, K., and Onishi, T., *J. Chem. Soc., Faraday Trans. I* **84**, 511 (1988).
15. Guglielminotti, E., *Langmuir* **6**, 1455 (1990).
16. Bianchi, D., Chafik, T., Khalfallah, M., and Teichner, S. J., *Appl. Catal. A* **123**, 89 (1995).
17. Wiegel, J., Koeppel, R. A., Baiker, A., and Wokaun, A., *Langmuir* **12**, 5319 (1996).
18. Ouyang, F., Kondo, J. N., Maruya, K., and Domen, K., *J. Phys. Chem. B* **101**, 4867 (1997).
19. Fisher, I. A., and Bell, A. T., *J. Catal.* **172**, 222 (1997).
20. Fisher, I. A., and Bell, A. T., *J. Catal.* **184**, 357 (1999).
21. Lavalley, J. C., *Catal. Today* **27**, 377 (1996).
22. Busca, G., *Catal. Today* **27**, 457 (1996).
23. He, M.-Y., and Ekerdt, J. G., *J. Catal.* **87**, 381 (1984).
24. Hertl, W., *Langmuir* **5**, 96 (1989).
25. Cerrato, G., Bordiga, S., Barbera, S., and Morterra, C., *Surf. Sci.* **50**, 50 (1997).
26. Morterra, C., Giamello, E., Orio, L., and Volante, M., *J. Phys. Chem.* **94**, 3111 (1990).
27. Bolis, V., Morterra, C., Volante, M., Orio, L., and Fubini, B., *Langmuir* **6**, 695 (1990).
28. Morterra, C., Bolis, V., Fubini, B., Orio, L., and Williams, T. B., *Surf. Sci.* **251/252**, 540 (1991).
29. Bolis, V., Morterra, C., Fubini, B., Ugliengo, P., and Garrone, E., *Langmuir* **9**, 1521 (1993).
30. Bolis, V., Cerrato, G., Magnacca, G., and Morterra, C., *Thermochim. Acta* **312**, 63 (1998).
31. Fisher, I. A., and Bell, A. T., *J. Catal.* **178**, 153 (1998).
32. Pokrovski, K., Jung, K. T., and Bell, A. T., *Langmuir* **17**, 4297 (2001).
33. Yildirimayan, H., and Gattow, G. Z., *Anorg. Allg. Chem.* **521**, 135 (1985).
34. Kaupp, G., Matthies, D., and de Verse, C., *Chem.-Zitg.* **113**, 219 (1989).
35. Tret'yakov, N. E., Pozdnaykov, D. E., Oranskaya, O. M., Filimonov, V. N., and Russ. J., *Phys. Chem.* **44**, 596 (1990).
36. Morterra, C., and Orio, L., *Mater. Chem. Phys.* **24**, 247 (1990).
37. Bianchi, D., Chafik, T., Khalafallah, M., and Teichner, S. J., *Appl. Catal.* **112**, 57 (1994).
38. Bianchi, D., Chafik, T., Khalafallah, M., and Teichner, S. J., *Appl. Catal.* **112**, 219 (1994).
39. Chafik, T., Bianchi, D., and Teichner, S. J., *Topics Catal.* **2**, 103 (1995).
40. Lamotte, J., Saur, O., Lavalley, J. C., Busca, G., and Lorenzelli, V., *J. Chem. Soc., Faraday Trans. I* **82**, 3019 (1986).
41. Cotton, F. A., and Wilkinson, G., "Advanced Inorganic Chemistry," 4th ed. Wiley, New York, 1980.
42. Arunasalam, V. C., Baxter, I., Darr, J. A., Drake, S. R., Hursthouse, M. B., Malik, K. M. A., and Mingos, D. M. P., *Polyhedron* **17**, 641 (1998).
43. Ouyang, F., Nakayama, A., Tabada, K., and Suzuki, E., *J. Phys. Chem. B* **104**, 2012 (2000).
44. Argon, P. A., Fuller, E. L., and Holmes, H. F., *J. Colloid Interface Chem.* **52**, 553 (1975).
45. Orlando, R., Pisani, C., Ruiz, E., and Sutet, P., *Surf. Sci.* **275**, 482 (1992).